ACS OMEGA

Open Access

http://pubs.acs.org/journal/acsodf

Article

Comparison of Cell-Penetrating and Fusogenic TAT-HA2 Peptide Performance in Peptideplex, Multicomponent, and Conjugate siRNA Delivery Systems

Metin Uz,* Volga Bulmus, and Sacide Alsoy Altinkaya

Cite This: *ACS Omega* 2024, 9, 47461−47474

Read Online

ACCESS | Metrics & More | Article Recommendations | Supporting Information

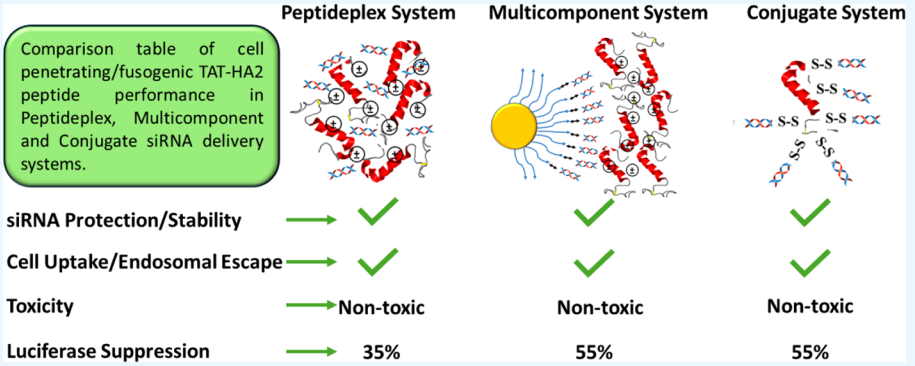

ABSTRACT: In this study, the performance of the cell-penetrating and fusogenic peptide, TAT-HA2, which consists of a cell-permeable HIV trans-activator of transcription (TAT) protein transduction domain and a pH-responsive influenza A virus hemagglutinin protein (HA2) domain, was comparatively evaluated for the first time in peptideplex, multicomponent, and conjugate siRNA delivery systems. TAT-HA2 in all three systems protected siRNA from degradation, except in the conjugate system with a low Peptide/siRNA ratio. The synergistic effect of different peptide domains enhanced the transfection efficiency of multicomponent and conjugate systems compared to that of peptideplexes, which was attributed to the surface configuration of TAT-HA2 peptides depending on the nature of attachment. Particularly, the multicomponent system showed better cellular uptake and endosomal escape than the peptideplexes, resulting in enhanced siRNA delivery in the cytoplasm. In addition, the presence of cleavable disulfide bonds in multicomponent and conjugate systems promoted the effective siRNA delivery in the cytoplasm, resulting in improved gene silencing activity. The multicomponent system reduced the level of luciferase expression in SKOV3 cells to 45% (±4). In contrast, the conjugate system and the commercially available siRNA transfection agent, Lipofectamine RNAiMax, caused luciferase suppression down to 55% (±2) at a siRNA dose of 100 nM. For the same dose, the peptideplex system could only reduce the luciferase expression to 65% (±5). None of the developed systems showed significant toxicity at any dose. Overall, the TAT-HA2 peptide is promising as a siRNA delivery vector; however, its performance depends on the nature of attachment and, as a result, its surface configuration on the developed delivery system.

1. INTRODUCTION

Small interfering RNA (siRNA), which acts in the cytoplasm by inhibiting the homologous mRNA (mRNA), is a promising agent for cancer treatment.[1−7] The success of this interference mechanism depends on efficient siRNA delivery to the cytoplasm, which requires overcoming various barriers, such as siRNA condensation and protection, stability, selective targeting, cellular entry, endosomal escape, and efficient siRNA release.[1,2,5,6,8,9] Over the past decade, various siRNA delivery systems, involving electrostatic complexation,[9−16] cleavable chemical bonds,[9,14,15,17,18] and a combination of the two,[19−21] have been developed based on various materials, such as polymers, inorganic nanoparticles, and peptides.[9,14−16,18,22−29] Among different materials, the combination of cell-penetrating peptide sequences with fusogenic peptides can be a promising alternative to design novel siRNA delivery systems, not only providing siRNA protection and stability but also enhancing cellular entry and endosomal escape, leading the cargo to the cytoplasm.[30,31] In this study, the commercial TAT-HA2 peptide, where a 10 amino acid cell-permeable HIV trans-activator of transcription (TAT) protein transduction domain (PTD) was

Received: June 21, 2024
Revised: November 1, 2024
Accepted: November 12, 2024
Published: November 20, 2024

attached to the first 20 amino acid sequence of influenza A virus hemagglutinin protein (HA2), was utilized.[32] The TAT domain provides cellular entry by binding to the cell surface and penetrating the membrane via lipid raft-dependent micropinocytosis, while the HA2 domain, which is a pH-sensitive lipid membrane destabilizing sequence, provides escape from macropinosomes and enhances transduction of the fusion peptide.[32−34] TAT and HA2 peptides have been used separately or in combination to design potential delivery vectors for various macromolecular therapeutics.[35−37] However, a comparative study for the use of the TAT-HA2 peptide combination in different systems as a carrier for siRNA delivery has not been reported yet. This study aims to fill the gap in the literature regarding detailed investigation of the TAT-HA2 peptide as a potential siRNA delivery vector in the form of complex, multicomponent, and conjugate systems. The peptide was attached to siRNA electrostatically (peptideplex) or covalently through cleavable disulfide bonds (conjugate). The multicomponent system (MCS) based on a gold nanoparticle (AuNP)−siRNA/Peptide combination was formed utilizing electrostatic interactions and chemical conjugations. Formation of each delivery system, siRNA loading, and stability were characterized by various techniques. In addition, each system's toxicity, cellular uptake, endosomal escape, and transfection efficiencies were evaluated in vitro using luciferase expressing SKOV3 ovarian cancer cells. This study shows that TAT-HA2 peptide-based siRNA delivery systems can be promising depending on the peptide's attachment method and surface configuration.

2. MATERIALS AND METHODS

2.1. Materials. Sodium citrate, sodium borohydrate, and hydrogen tetrachloroaurate (III) trihydrate (99.9%) were obtained from Sigma-Aldrich for gold nanoparticle preparation. Thiol and amine end group-modified bifunctional PEG (SH-PEG-NH_2: MW1000) and the *N*-succinimidyl 3-(2-pyridyldithio)-propionate (SPDP) cross-linker for gold nanoparticle surface modification were obtained from Creative PEGworks and Thermo Scientific, respectively. The luciferase-suppressing nonthiol-modified and thiol-modified siRNA sequences (sense: 5′ HS-GAUUAUGUCCGGUUAUGUA-UU 3′; antisense: 5′ UACAUAACCGGACAUAAUC-UU 3′) were purchased from IDT-DNA Technologies. The cell-penetrating and fusogenic peptide, TAT-HA2, was obtained from Anaspec (RRRQRRKKRGGDIMGEWGNEIFGAIAGFLG). The luciferase expressing ovarian cancer cell line, SKOV3 (AKR-232), was purchased from Creative Biogene. All the cell culture media and supplements (i.e., Dulbecco's modified Eagle medium (DMEM), fetal bovine serum (FBS), penicillin−streptomycin (PenStrep), L-glutamine, and nonessential amino acids (NEAA)) were purchased from Invitrogen. The lysosome staining fluorescence dye, Lysotracker Red, NHS-FITC fluorescence (5/6-carboxyfluorescein succinimidyl ester) dye for peptide labeling, and a Quanti Ribogreen siRNA detection kit were purchased from Invitrogen. The CellTiter96 for MTT and Luciferase assay kit for luciferase detection were purchased from Promega. Polyacrylamide gel desalting columns (MWCO: 1800) were obtained from Invitrogen.

Sterile RNase-free water was used in preparing all of the buffers used in the experiments by following standard laboratory procedures.

2.2. Preparation of Peptide/siRNA Complex Systems (Peptideplexes). Peptide/siRNA complexes (peptideplexes) at different molar ratios of nitrogen (N) in the TAT-HA2 peptide to phosphate (P) in siRNA were obtained by mixing the appropriate quantities of peptide solution in PBS at pH 7.4 with the siRNA solution (1 μL of 100 μM siRNA stock solution in RNase free water). The Peptide/siRNA molar ratio was adjusted to 1.25, 2.5, 5, 7.5, 10, and 12.5, which also corresponds to the N/P molar ratio since there are ∼40 mol of nitrogen per 1 mol of peptide and ∼40 moles of phosphates per 1 mol of siRNA. To enable electrostatic complexation, the mixture was incubated at room temperature for 30 min. The siRNA condensation and peptideplex formation were confirmed on a 2% (w/v) agarose gel containing 0.5 μg/mL of ethidium bromide (EtBr). The samples were run in the gel for 30 min at 100 V in 1x TAE buffer. The electrophoretic mobility of the polyplexes was imaged by using a UV-transilluminator.

2.3. Preparation of Multicomponent Systems (MCSs). The AuNP and peptide-based multicomponent system was prepared by following a similar procedure as described in our previous work.[19] Briefly, the ∼13 nm gold nanoparticles were prepared using a citrate reduction method as described elsewhere.[38] In the second step, the surface of AuNPs (10 nM concentration) was modified with a heterobifunctional PEG molecule (1 mg/mL of thiol-PEG-amine, SH-PEG-NH_2) through gold−sulfur bonds[39] in order to facilitate subsequent surface modifications. Following the PEG attachment, an amine and sulfhydryl reactive heterobifunctional cross-linker (1 mM SPDP, *N*-succinimidyl 3-(2-pyridyldithio)-propionate), was mixed with 10 nM AuNP-PEG solution in equal amounts prior to siRNA attachment. The thiol-modified siRNA was deprotected via TCEP (tris(2-carboxyethyl)phosphine) reduction as described in the manufacturer's protocol (IDT-DNA). Then, the AuNP-PEG-SPDP conjugate was modified with deprotected thiol-modified siRNA via cleavable disulfide bonds through thiol−disulfide exchange reaction.[19] After the conjugation, the loaded amount of siRNA was quantified using a Quant-iT Ribo Green siRNA detection kit by following the manufacturer's procedure. The surface of siRNA attached AuNPs was electrostatically coated with a positively charged peptide to obtain a AuNP-siRNA-Peptide multicomponent system. An appropriate amount of peptide was mixed with a 20 nM AuNP-PEG-siRNA conjugate in phosphate buffer (PBS) at pH 7.4 and incubated 20 min at room temperature. The molar ratio of AuNP/Peptide was varied as 1/125, 1/250, and 1/500, which correspond to Peptide/siRNA molar ratios of 1.25, 2.5, and 5, respectively. At the end of each step, the modified AuNPs were centrifuged at 20000 *g* for 15 min and washed with PBS four times to eliminate weakly bound surface components.

The AuNPs after each modification step were characterized using different techniques. The changes in size, size distribution, and zeta potential of the AuNPs were determined by dynamic light scattering (DLS) (Malvern Zetasizer Nanozs90). The red shift in the specific wavelength of bare AuNPs (520 nm for ∼13 nm AuNPs), at which maximum absorption was observed, was also used to verify the modification of AuNPs' surface via a UV−vis spectrophotometer (PerkinElmer Lambda 45).

2.4. Preparation of Peptide−siRNA Conjugate Systems. In this strategy, siRNA was conjugated to the peptide through cleavable disulfide bonds. First, a peptide solution (115 μM in PBS at pH7.4) was mixed with an SPDP cross-linker (25 μL of SPDP solution in 20 mM, 10% DMSO in PBS-EDTA). After 3 h of continuous stirring at room temperature, the unreacted SPDP was removed from the mixture through a polyacrylamide gel desalting column (molecular weight cut off

https://doi.org/10.1021/acsomega.4c05808
ACS Omega 2024, 9, 47461−47474

Scheme 1. Schematic Representation of the Developed Systems[a]

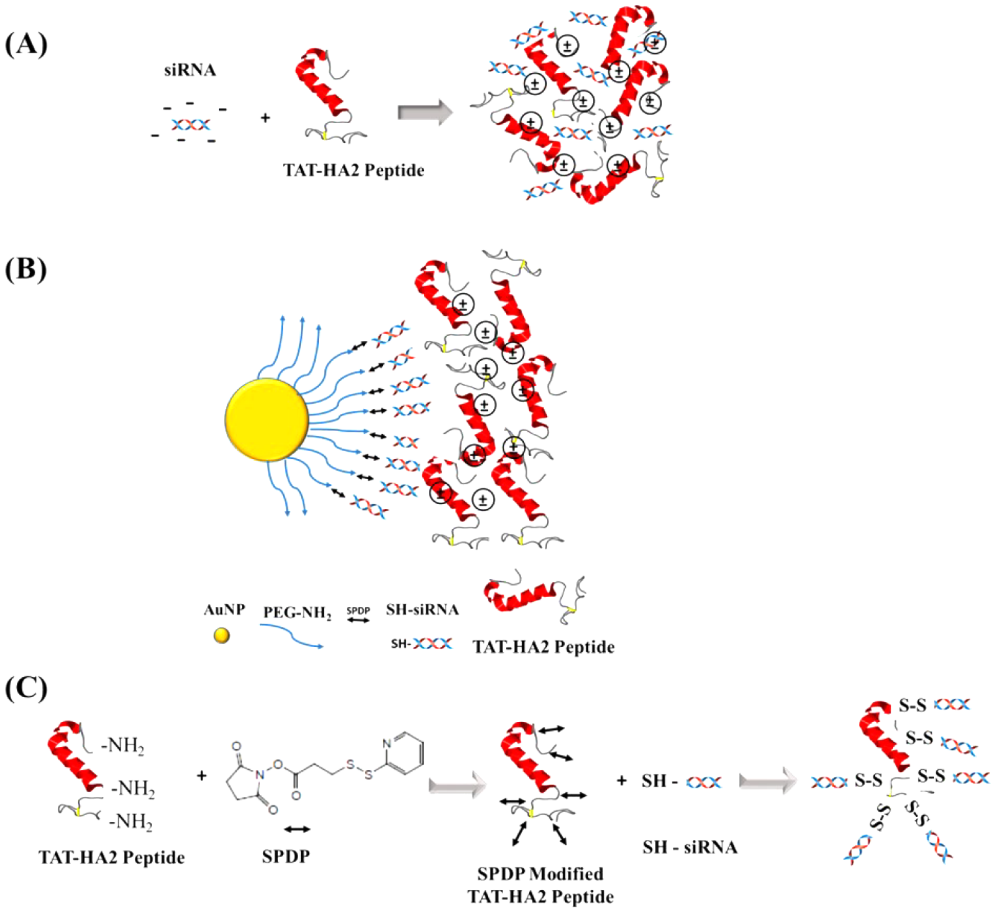

[a](A) Peptideplexes. (B) Gold nanoparticle-based multicomponent system (MCS). (C) Conjugate system.

(MWCO), 1.8 kDa). The SPDP-modified peptides, collected from the column, were concentrated in a speed vacuum evaporator and further reacted with DTT (dithiothreitol) to deprotect the 2-pyridyldithio group of the cross-linker. The concentration of the released pyridine-2-thione was measured using a UV−vis spectrophotometer at 343 nm to determine the SPDP modification degree (Supporting Information). Following SPDP modification, the thiol-modified siRNA was attached to the peptide through the disulfide exchange reaction. For this purpose, different amounts of peptide solution (115 μM in PBS at pH 7.4) were reacted with a 20 μM siRNA solution in borate buffer (2.5 M NaCl, 30 mM borate, pH 8.5, 0.01% Tween 20) for 48 h at room temperature. The molar ratio of peptide to siRNA was changed to 5, 7.5, and 10. Then, the obtained conjugates were purified using dialysis (Spectra Por 129120 Biotech-Grade RC Dialysis Tubing, 15 kDa MWCO) and were further concentrated using a speed vacuum evaporator. The successful Peptide−siRNA conjugation was determined by exposing the achieved Peptide−siRNA conjugates to TCEP to cleave the disulfide bonds and release the conjugated siRNA in a dialysis bag (MWCO = 5 kDa). The dissociated peptide (MW 3433 Da) diffuses out through the dialysis bag, while the cleaved siRNA (MW 13600 Da) remains within the dialysis tube, and its amount was determined using the Quant-iT Ribo Green siRNA detection kit following the manufacturer's procedure. The Peptide−siRNA conjugation was also visualized by agarose gel electrophoresis as mentioned in Section 2.2.

2.5. Characterization and Performance Evaluation of Developed Systems. *2.5.1. RNase and Serum Protein Stability of the Systems.* The mobility of siRNA in gel electrophoresis was used to determine the protective effect and stability of the developed systems (peptideplex, multicomponent, and conjugate) against RNase and serum proteins. The PBS containing 0.25% RNase or 50% serum was used as the medium to test the stability of the developed systems at 37 °C for 6 h. After the incubation, the gel electrophoresis was performed as mentioned in Section 2.2. In addition, the size and zeta potential stabilities of the developed systems in PBS and serum-containing cell culture media (DMEM) were observed by dynamic light scattering (DLS).

2.5.2. Cellular Uptake and Accumulation of Prepared Systems. The luciferase-expressing SKOV3 cells were grown in high-glucose DMEM, supplemented with 10% (v/v) FBS, 0.1 mM NEAA, 2 mM L-glutamine, and 1% Pen-Strep, at 37 °C under a humidified atmosphere containing 5% CO_2, and were passaged every 2−3 days.

The time-dependent cellular uptake and accumulation of peptideplexes were evaluated through flow cytometry analysis. For this purpose, the peptides were first labeled with a NHS-Fluorescein dye by following the manufacturer's procedure. Peptide solution (1 mg/mL) in 50 mM borate buffer at pH 8.5 was reacted with NHS-FITC (1 mg/mL) in dimethyl sulfoxide (DMSO) for 3 h. Then, the unreacted dye was removed through a polyacrylamide gel desalting column, and the collected samples were concentrated in a speed vacuum evaporator. The

https://doi.org/10.1021/acsomega.4c05808
ACS Omega 2024, 9, 47461−47474

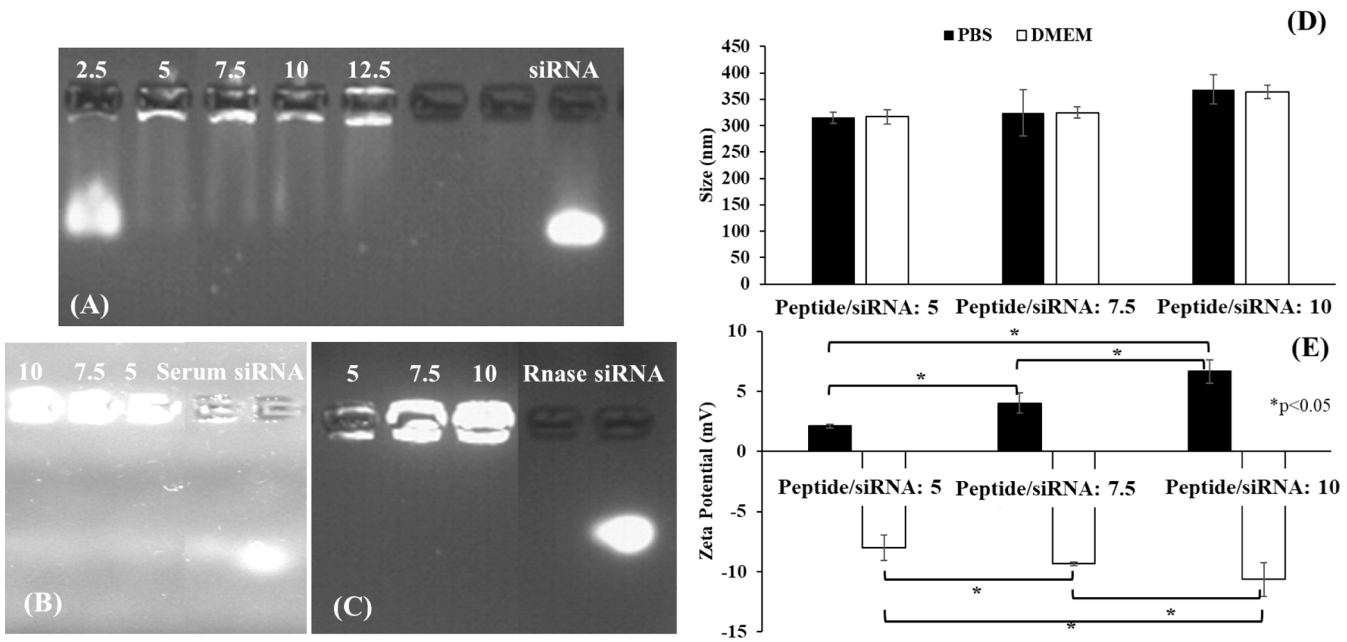

Figure 1. (A) Gel electrophoresis of siRNA/Peptide complexes formed at various Peptide/siRNA ratios: 2.5, 5, 7.5, 10, and 12.5. Control: naked siRNA. (B) Serum stability of the siRNA/Peptide complexes formed at Peptide/siRNA ratios of 5, 7.5, and 10. Serum content: 50% (v/v). Incubation: 6 h at 37 °C. (C) RNAse-exposed siRNA/Peptide complexes at various Peptide/siRNA ratios: 5, 7.5, 10. Control: naked siRNA and RNase exposed naked siRNA. RNase concentration: 0.25% (v/v). Incubation: 6 h at 37 °C. The size (D) and zeta potential (E) values of siRNA/Peptide peptideplexe systems (Peptide/siRNA ratio: 5, 7.5, and 10) measured immediately in PBS or after 24-h incubation in a serum-containing DMEM growth medium. * represents a statistically significant difference ($p < 0.05$).

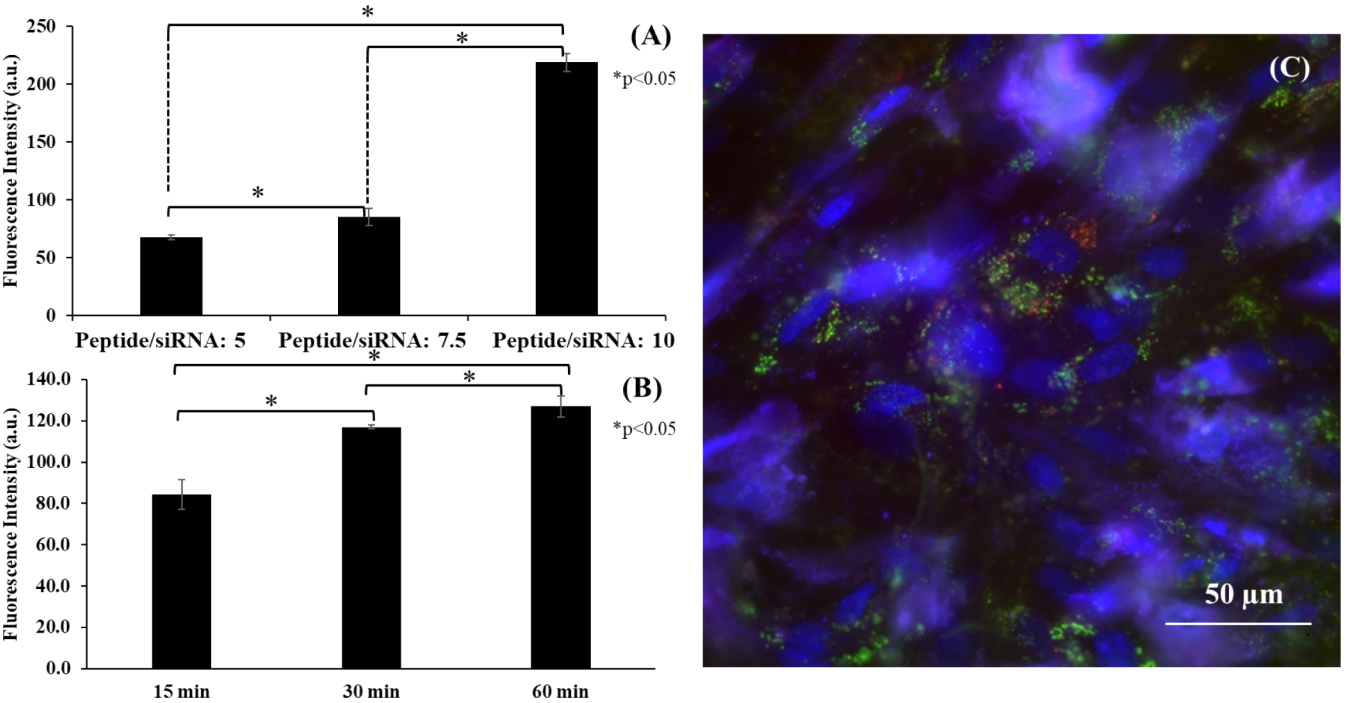

Figure 2. (A) The cellular accumulation of peptideplexes at different Peptide/siRNA ratios. Incubation time: 24 h. (B) Time-dependent cellular uptake of siRNA/Peptide peptideplexes (Peptide/siRNA ratio: 10). Applied dose: 100 nM based on siRNA. Incubation times: 15, 30, and 60 min. * represents a statistically significant difference ($p < 0.05$). (C) Merged fluorescence images of siRNA/Peptide complexes prepared with a Peptide/siRNA ratio of 10. Green: peptideplexes stained by FITC, Red: Lysosome stained by LysotrackerRed, Blue: Nucleus stained by DAPI. Incubation time: 24 h.

labeling degree of the peptide was calculated as shown in the Supporting Information. The peptideplexes were then prepared by using dye-attached peptides as described in Section 2.2. SKOV3 cells (2×10^5 cells/well) were exposed to peptideplexes prepared at various N/P ratios and incubated at 37 °C under a 5% CO_2 atmosphere for 24 h. At the end of the incubation, the cells were harvested, and the cellular uptake was determined by

https://doi.org/10.1021/acsomega.4c05808
ACS Omega 2024, 9, 47461−47474

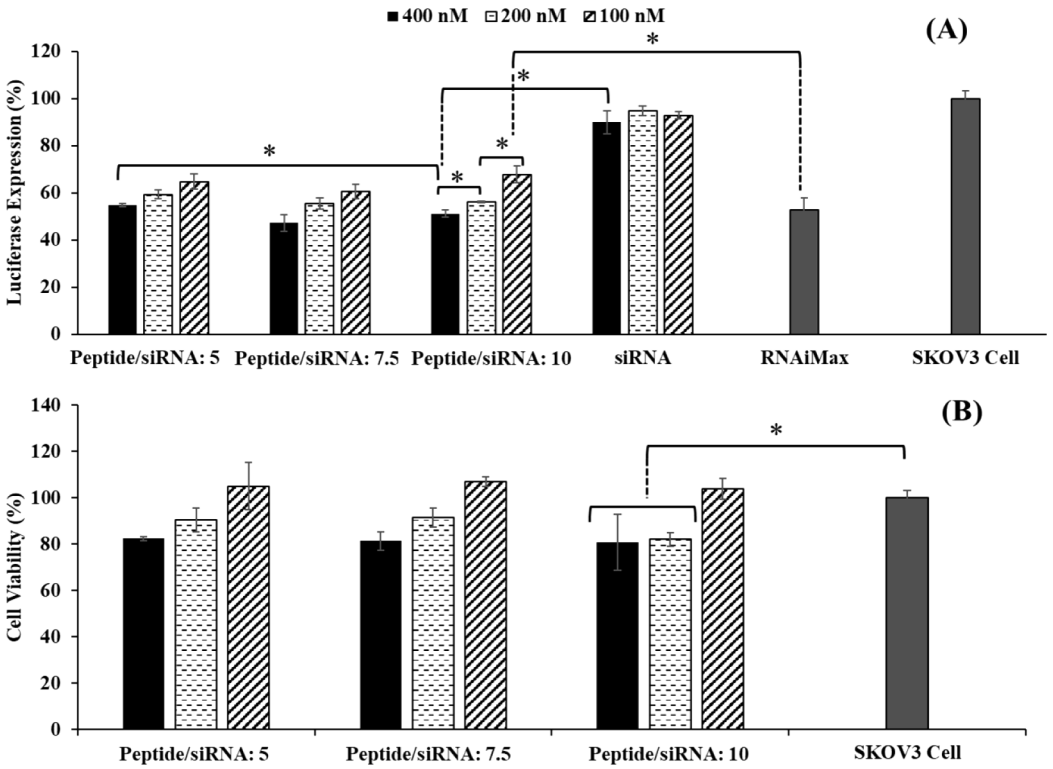

Figure 3. (A) Luciferase expression suppression and (B) cell viability of the prepared siRNA/Peptide complexes administered to SKOV3 cells. Peptide/siRNA: 5, 7.5, and 10. Applied siRNA dose: 100, 200, and 400 nM. Commercial Lipofectamine RNAiMax siRNA transfection reagent with a 100 nM siRNA dose. Initial SKOV3 cell density: 1×10^4 cells/well. Incubation time: 24 h. * represents a statistically significant difference ($p < 0.05$) between the selected cases.

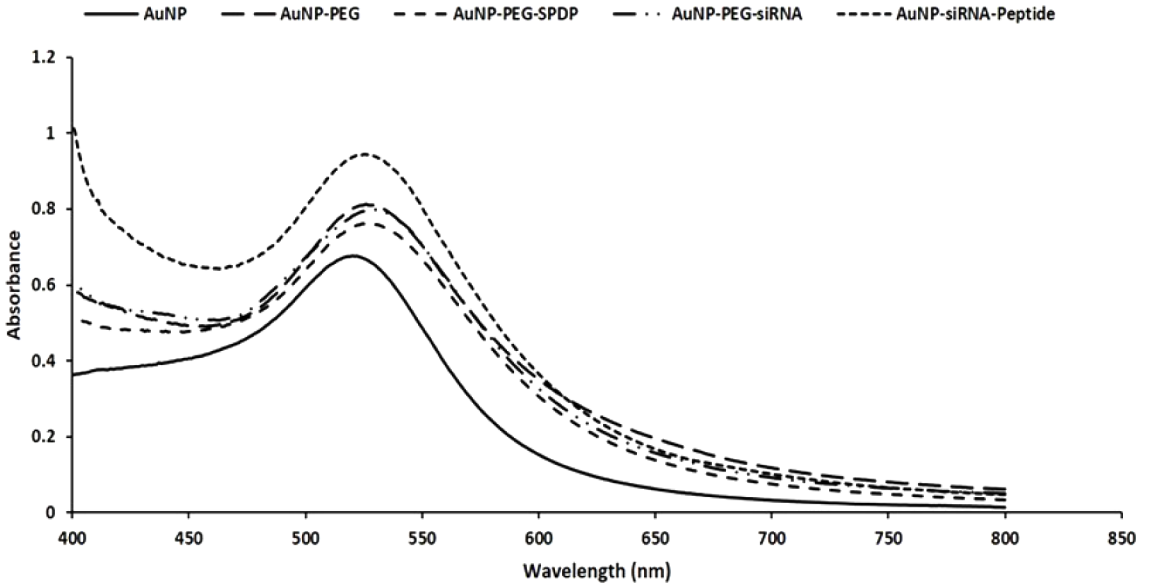

	Bare AuNP	AuNP-PEG	AuNP-PEG-SPDP	AuNP-PEG-siRNA	AuNP-siRNA-Peptide
Size (nm)	12.5 ±0.7	18.1 ±0.6	20.4 ±0.9	31.8 ±0.1	46 ±2
PDI	0.23	0.25	0.24	0.25	0.34
Zeta Potential (mV)	-33.3 ±1	20.2 ±1.2	3.9 ±1.5	-2.6 ±0.7	5 ±0.3

Figure 4. UV−vis spectra of AuNP, PEG-modified AuNP, SPDP, and siRNA-modified AuNP-PEG, and peptide-coated AuNP-siRNA multilayer system (AuNP/Peptide ratio: 1/500 or Peptide/siRNA ratio: 5 is shown here since all other ratios showed a similar trend).

https://doi.org/10.1021/acsomega.4c05808
ACS Omega 2024, 9, 47461−47474

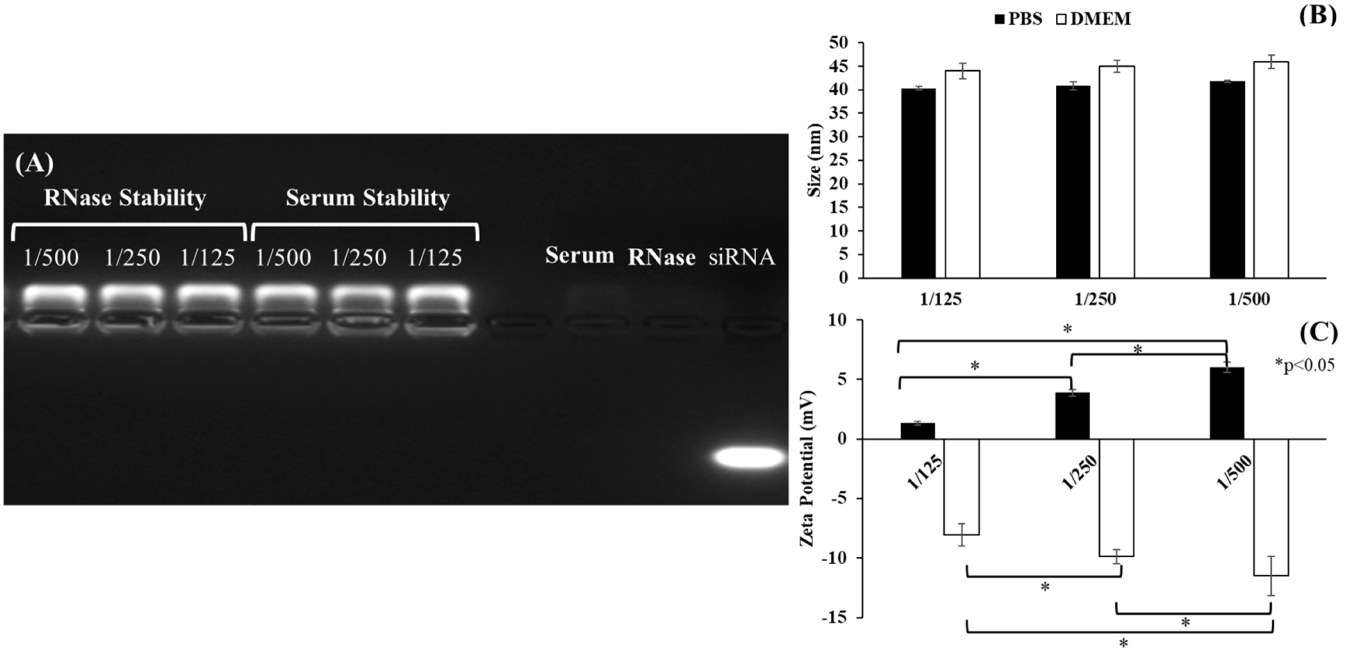

Figure 5. (A) Agarose gel electrophoresis of the AuNP-siRNA-Peptide MCS and naked siRNA. RNase and serum stabilities of the MCSs were prepared at AuNP/Peptide ratios of 1/125, 1/250 and 1/500 (Peptide/siRNA ratios of 1.25, 2.5, and 5, respectively) Serum content: 50% (v/v). Incubation: 6 h at 37 °C. RNase concentration: 0.25% (v/v). Incubation: 1 h at 37 °C. The change in the size (B) and zeta potential (C) values of AuNP-siRNA-Peptide MCSs (AuNP/Peptide ratios: 1/125, 1/250, and 1/500 or Peptide/siRNA ratios: 1.25, 2.5, and 5) after preparation in PBS buffer (PBS) and after 24 h of incubation at 37 °C in serum-containing DMEM growth medium (DMEM). * represents a statistically significant difference ($p < 0.05$).

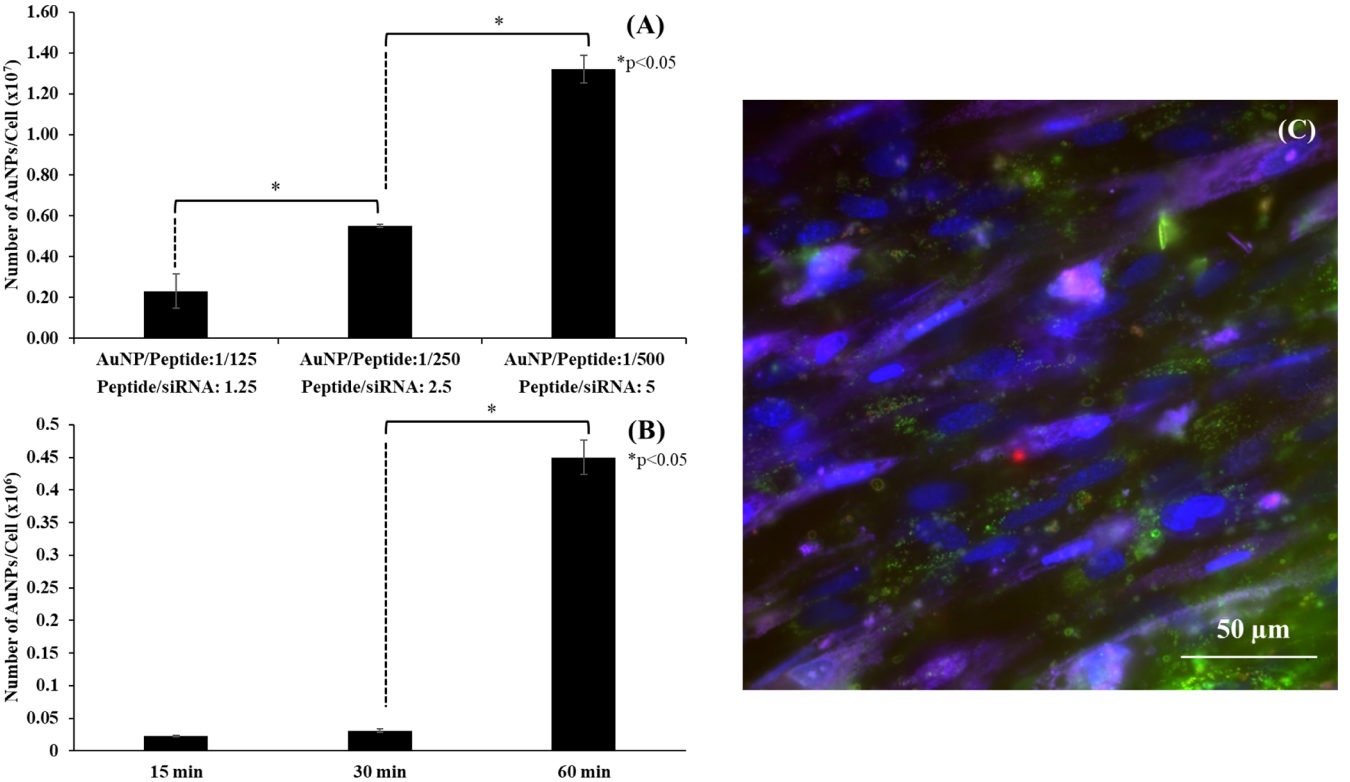

Figure 6. (A) The cellular accumulation of AuNP-based MCSs in SKOV3 cells measured by ICP-MS. Applied dose based on siRNA amount: 100 nM. Incubation time: 24 h. (B) Time-dependent cellular uptake of AuNP-siRNA-Peptide MCSs (AuNP/Peptide ratio: 1/500 or Peptide/siRNA ratio: 5). Applied dose: 100 nM based on siRNA. Time: 15, 30, and 60 min. * represents a statistically significant difference ($p < 0.05$). (C) Fluorescence images of AuNP-siRNA-Peptide MCSs prepared with a AuNP/Peptide ratio of 1/500 (Peptide/siRNA ratio of 5). Applied dose: 100 nM based on siRNA. Green: MCSs stained by FITC, Red: Lysosome stained by LysotrackerRed, Blue: Nucleus stained by DAPI.

https://doi.org/10.1021/acsomega.4c05808
ACS Omega 2024, 9, 47461−47474

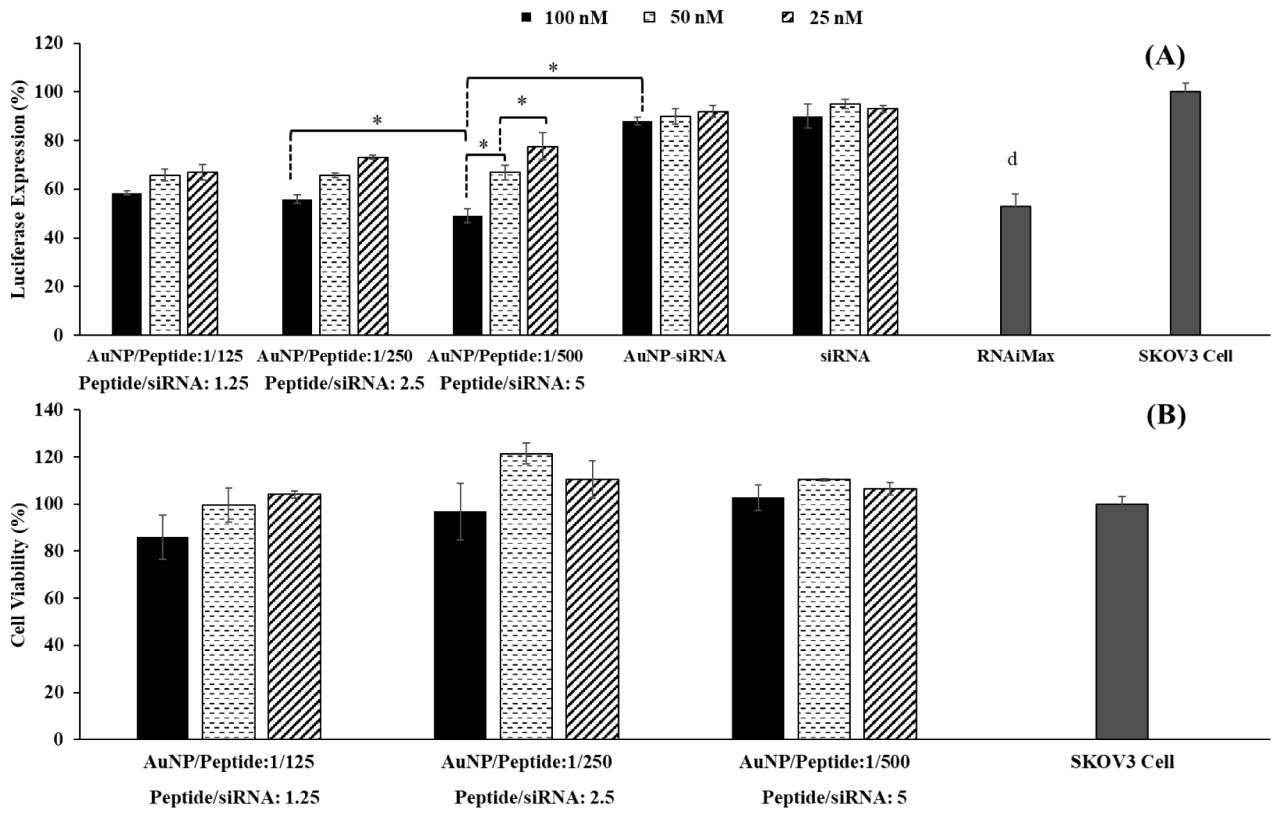

Figure 7. (A) Luciferase suppression and (B) cell viability of prepared AuNP-siRNA-Peptide MCSs (AuNP/Peptide ratio: 1/125, 1/250, and 1/500 or Peptide/siRNA ratio: 1.25, 2.5, and 5, respectively). Applied siRNA dose: 100, 50, 25 nM/well. Commercial Lipofectamine RNAiMax siRNA transfection reagent with 100 nM siRNA dose. Initial SKOV3 cell density: 1×10^4 cells/well. Incubation time: 24 h. * represents a statistically significant difference ($p < 0.05$) between the selected cases.

flow cytometer (BD Biosciences FACSCanto) by detecting the fluorescence intensity of the peptideplexes within the cells.

The cellular uptake and accumulation of multicomponent systems were evaluated through inductively coupled plasma mass spectroscopy (ICP-MS) analysis. SKOV3 cells (2×10^5 cells/well) were seeded and incubated with MCSs at 37 °C in a 5% CO_2 humidified incubator for 24 h. After incubation, the cell culture medium was removed, and the cells were washed with PBS to remove the excess nanoparticles in the medium or the nanoparticles that adhered to the cell membrane. Then, the cells were harvested, and the cell pellet was obtained via centrifugation. The AuNPs in the cells were digested by treating the cell pellet with 500 μL of concentrated nitric acid (HNO_3) at 70 °C for 4 h.[40] ICP-MS (Agilent 7500ce) was used to determine the quantity of gold in the cells, and the number of AuNPs per cell was calculated as described in the Supporting Information.

The cellular uptake and accumulation of conjugate systems could not be evaluated since successful fluorescein staining could not be achieved in this case. We think that the prior occupation of available groups in the peptide structure with siRNA prevented efficient fluorescein staining and further flow cytometry analysis.

2.5.3. Cell Uptake by Fluorescence Microscopy. The fluorescence microscope images were obtained for the peptideplexes and MCS prepared using the fluorescent dye-attached to the peptide (described in Section 2.5.2.). Both systems were incubated with the SKOV3 cells (initial cell seeding density: 2×10^5 cells/well) for 24 h at 37 °C under a 5% CO_2 atmosphere. The cells were then stained with LysoTracker Red and DAPI per the manufacturer's procedure and analyzed through fluorescence microscopy.

2.5.4. Cytotoxicity Tests. To evaluate the toxicities of the developed systems, SKOV3 cells were plated at a density of 1×10^4 cells/well in 96-well plates. After the cells reached confluency at the end of 24 h, different siRNA formulations were applied at varying doses, and cells were further incubated for 24 h. Following incubation, a CellTiter 96 assay kit was used as per the manufacturer's procedure to detect the toxicity.

2.5.5. Luciferase Activity Test. The SKOV3 cells were grown in 96-well plates with a seeding density of 2×10^4 cells/well for 24 h. Then, the developed nano formulations at various concentrations were administered to the wells and incubated for 24 h under the same conditions. Following the incubation, the Luciferase assay kit procedure was applied per the manufacturer's instructions. Briefly, the cells were treated with 20 μL of 1X lysis buffer, and the plate was placed into the multimode plate reader (Thermo Scientific, Varioskan Multimode Microplate Reader). The change in luciferase expression values was recorded in luminescence mode following the instant injection of 100 μL of Luciferase Assay Reagent into each well. The commercial RNAiMax siRNA transfection reagent was used as a control by following the manufacturer's protocol.

2.5.6. Statistical Analysis. The ANOVA analysis by Tukey's method with a 95% confidence interval was used to evaluate the statistical significance between the experimental groups. At least three independent experiments were used to calculate the mean and standard deviations to present the results.

https://doi.org/10.1021/acsomega.4c05808
ACS Omega 2024, 9, 47461−47474

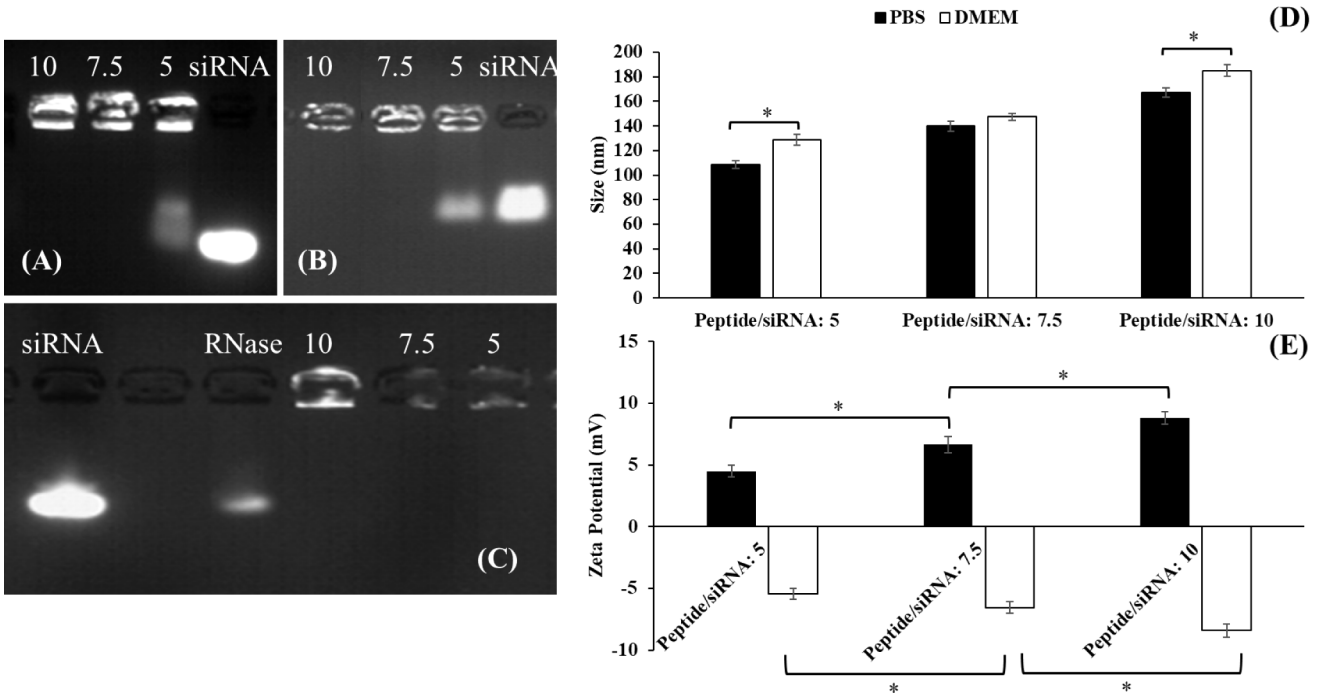

Figure 8. (A) Gel electrophoresis of Peptide−siRNA conjugates at various Peptide/siRNA ratios: 5, 7.5, and 10. Control: Naked siRNA. (B) Serum stability of the Peptide−siRNA conjugates at Peptide/siRNA ratios of 5, 7.5, and 10. Serum content: 50% (v/v). Incubation: 6 h at 37 °C. (C) RNase-exposed Peptide−siRNA conjugates at various Peptide/siRNA ratios: 5, 7.5, and 10. Control: naked siRNA and RNase-exposed naked siRNA. RNase concentration: 0.25% (v/v). Incubation: 1 h at 37 °C. The change in the size (D) and zeta potential (E) values of Peptide−siRNA conjugate systems (Peptide/siRNA ratios: 5, 7.5, and 10) after preparation in PBS buffer (PBS) and after 24 h of incubation at 37 °C in serum-containing DMEM growth medium (DMEM). * represents a statistically significant difference ($p < 0.05$) between the selected cases.

3. RESULTS AND DISCUSSION

In this study, the performances of three different formulations, the peptideplex system, AuNP containing multicomponent system, and conjugate system (Scheme 1), were evaluated and compared in terms of siRNA protection, stability, cellular uptake, endosomal escape, siRNA activity, and cytotoxicity against the luciferase-expressing SKOV3 cell line.

3.1. Peptide/siRNA Peptideplex System. Peptideplexes were obtained through direct electrostatic interactions between the positively charged groups of the peptide and the negatively charged phosphate groups of siRNA. The Peptide/siRNA molar ratio varied from 1.25 to 12.5; however, complete complexation between siRNA and peptide was achieved at ratios higher than 2.5 (Figure 1A). The siRNA's incomplete condensation was noted by the similar mobility of the naked siRNA on agarose gel with that of the siRNA condensed with the peptides when the Peptide/siRNA ratio was 2.5 (Figure 1A). As the Peptide/siRNA ratio increases, the electrostatic attachment between siRNA and peptide gets stronger, resulting in the complexation of all siRNA molecules and the formation of stable complexes. However, strong electrostatic interactions prevent the efficient siRNA release in the cytoplasm.[11−13,41] Considering these facts, we have selected the peptideplexes formed at the Peptide/siRNA ratios of 5, 7.5, and 10 for further investigation. (Figure 1A). In preliminary experiments, the peptideplex particles formed at varying Peptide/siRNA ratios (from 5 to 10) were dialyzed to determine whether there were free peptides that were not complexed with siRNA and released to dialyzate. The results showed that there were no free peptides in the peptideplex particle solutions prepared at Peptide/siRNA ratios of 5, 7.5, and 10.

The selected peptide complexes were exposed to serum proteins and RNase enzymes to determine the stability and siRNA protection provided by the peptide complexation. The peptideplexes formed at the Peptide/siRNA ratios of 7.5 and 10 did not dissociate in the presence of serum proteins after a 6-h incubation, whereas the Peptide/siRNA ratio of 5 resulted in weak electrostatic interactions, hence a slight dissociation (Figure 1B). The naked siRNA completely degraded in the presence of the RNase enzyme, showing no band on the gel, while the peptideplexes with Peptide/siRNA ratios of 7.5 and 10 provided efficient siRNA protection with significantly visible RNA bands (Figure 1C). A poor siRNA intensity was observed for the peptideplex with a Peptide/siRNA ratio of 5 probably due to relatively weaker electrostatic complexation between siRNA and peptide (Figure 1C).

The size and zeta potential of the peptideplexes were measured in PBS and a serum-containing DMEM growth medium after 24 h of incubation. The zeta potential values in PBS increased with the increased Peptide/siRNA ratio due to the higher amount of peptide in the complexes. (Figure 1D and E). After storing in DMEM, the zeta potential of the peptideplexes changed from positive to negative as a result of the adsorption of negatively charged serum components, such as albumin (Figure 1E). The size of peptideplexes in PBS or in DMEM did not change with the changing Peptide/siRNA ratio due to the small size of serum components (~7 nm)[42,43] compared to the size of peptideplexes (~300 nm).

The cellular accumulation, time-dependent cellular uptake, and endosomal escape capabilities of peptideplexes were evaluated through flow cytometry and fluorescence microscopy (Figure 2). The flow cytometry results showed that the cellular accumulation of peptideplexes prepared at a Peptide/siRNA

https://doi.org/10.1021/acsomega.4c05808
ACS Omega 2024, 9, 47461−47474

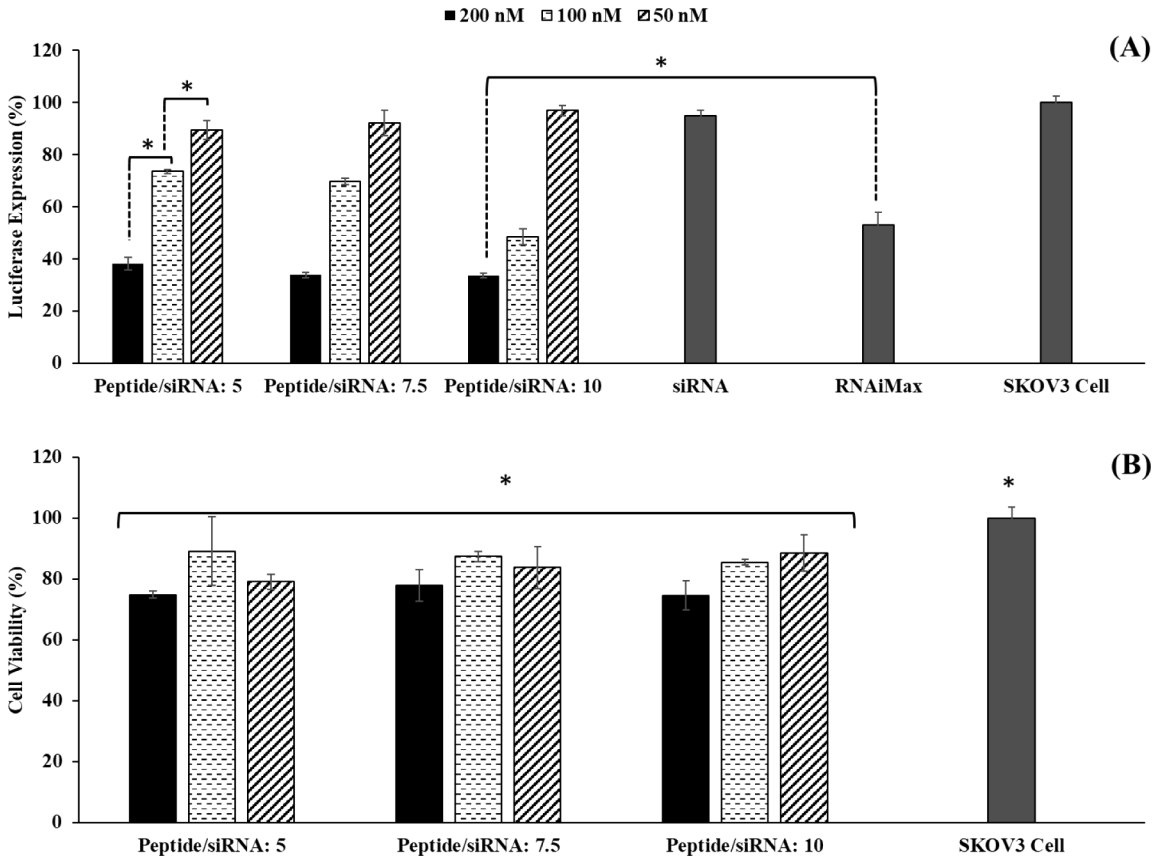

Figure 9. (A) Luciferase expression suppression and (B) cell viability of prepared Peptide−siRNA conjugates administered to SKOV3 cells. Peptide/siRNA ratios: 5, 7.5, and 10. Applied siRNA doses: 200, 100, and 50 nM. Commercial Lipofectamine RNAiMax siRNA transfection reagent with a 100 nM siRNA dose. Initial SKOV3 cell density: 1×10^4 cells/well. Incubation time: 24 h. * represents a statistically significant difference ($p < 0.05$) for selected cases.

ratio of 10 was significantly higher (Figure 2A). The time-dependent cellular uptake of this peptideplex reached almost a plateau within 60 min (Figure 2B). The TAT domain in the peptide enhances cellular entry and accumulation through arginine and lysine residues, which enhance cell membrane penetration.[44,45] Thus, an increasing amount of peptide in the structure is beneficial for accumulation.

It is known that following cellular entry, efficient endosomal escape is required to prevent degradation of siRNA in the endosome and show activity in the cytoplasm.[46] The intracellular distribution and endosomal escape capability of the prepared peptideplex were visualized by fluorescence microscopy (Figure 2C). It was observed that ∼55% of the peptideplexes escaped from the endolysosomal pathway and were released into the cytoplasm. ImageJ software quantified the amount of particles distributed within the cytoplasm over the total particle amount.

The HA2 domain of the peptide is the fusogenic component responsible for endosomal escape. At acidic pH, the conformational change to a helical structure occurs upon protonation of the glutamic acid and the aspartic acid in the HA2 domain, resulting in the destabilization of the endosomal membrane.[32,33,35,47,48] The poor endosomal escape of the peptideplexes could be due to the embedding of the active segments of the HA2 domain in the complex structure, preventing the interaction of the helical fusogenic structure with the endolysosomal membrane.

The peptideplexes formed at different Peptide/siRNA ratios (5, 7.5, and 10) were administered to the SKOV3 cells at variable doses, and their effect on luciferase expression and toxicity was determined (Figure 3). Compared to the control, all of the peptideplexes showed ∼50% suppression in luciferase expression at their maximum siRNA dose (400 nM) without showing severe toxicity (∼80% cell viability) (Figure 3). Reducing the dose from 400 to 100 nM decreased the luciferase suppression to ∼35% while increasing cell viability to ∼100%. The cell viability and luciferase activity were dose-dependent but not affected by the Peptide/siRNA ratio. Compared to previous studies published in the literature,[49−52] the biological activity of the Peptide/siRNA peptideplexes on luciferase expression was found to be moderate. At a 100 nM siRNA dose, the peptideplex prepared at a Peptide/siRNA ratio of 10 showed only ∼10% less luciferase suppression than its commercial counterpart RNAiMax (Figure 3A). The low performance of the peptideplexes could be due to strong electrostatic attraction between siRNA and peptide, providing stability but avoiding efficient siRNA release, hence, endolysosomal escape and activity in the cytoplasm.[30,53] Another reason might be the occupation of cationic arginine amino acids within the TAT domain with siRNA molecules or embedding glutamic acid and aspartic acid in the HA2 domain during the complexation with siRNA, which are both responsible components for cytoplasmic escape.[25] Although the change in the Peptide/siRNA ratio profoundly varied the cell uptake, these differences did not significantly affect luciferase expression and toxicity.

https://doi.org/10.1021/acsomega.4c05808
ACS Omega 2024, 9, 47461−47474

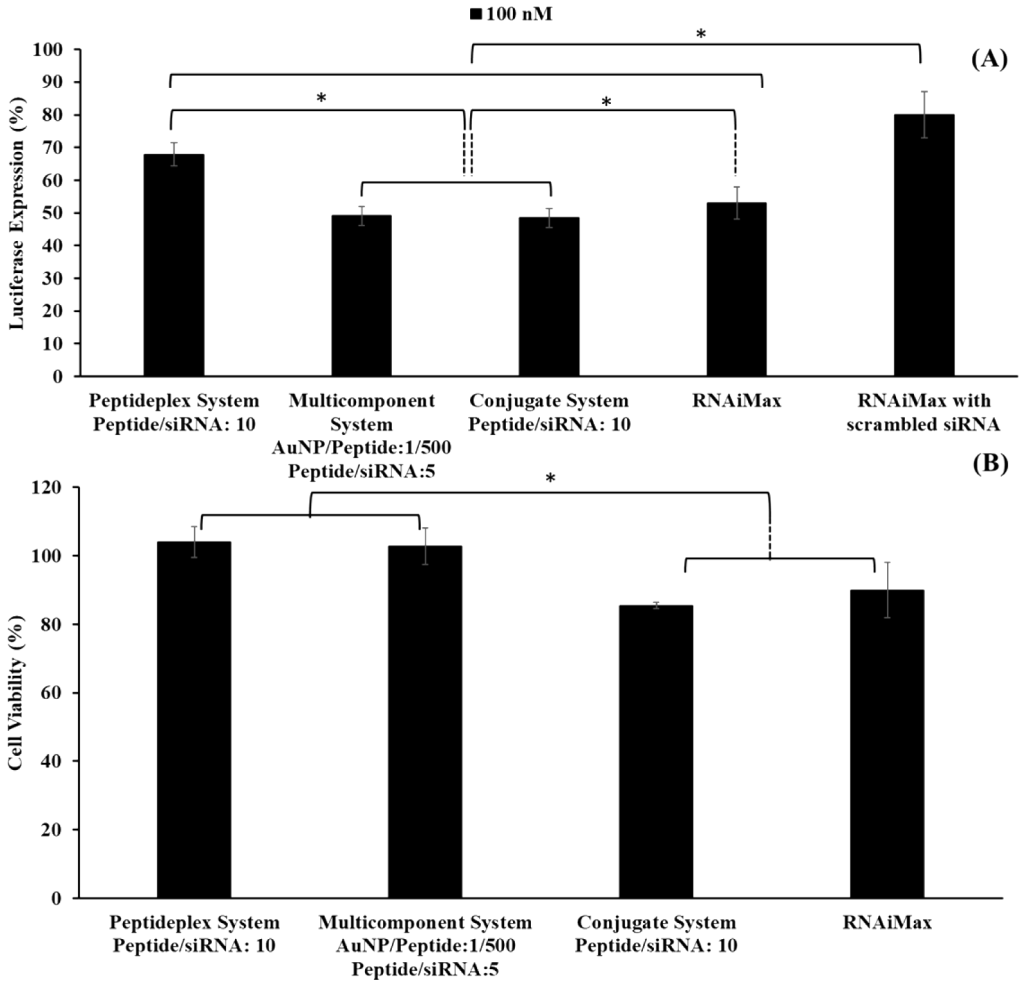

Figure 10. (A) Luciferase expression suppression and (B) cell viability of peptideplex, multicomponent, and conjugate systems administered to SKOV3 cells. The siRNA dose is 100 nM for all the systems. The positive control is the commercial Lipofectamine RNAiMax siRNA transfection reagent with a 100 nM siRNA dose. The negative control is the commercial Lipofectamine RNAiMax transfection reagent with scrambled siRNA at a 100 nM siRNA dose. Initial SKOV3 cell density: 1×10^4 cells/well. Incubation time: 24 h. * represents a statistically significant difference ($p < 0.05$) for selected cases.

3.2. AuNP, siRNA, and Peptide-Based Multicomponent System. As an alternative to the peptideplex systems, the AuNP and peptide-based multicomponent system was constructed based on electrostatic interactions and cleavable chemical bonds. The system was prepared using the same protocol followed in our previous work.[19] The first step in developing a multicomponent system (MCS) was the modification of AuNPs with heterobifunctional PEG to provide stability and additional conjugation sites for siRNA attachment through cleavable disulfide bonds. PEG coating resulted in an increase in the cumulative size of the AuNPs from ∼12.5 to ∼18 nm. It turned the negatively charged surface of the bare AuNPs (−33 mV) into a positively charged (+20 mV) surface due to the presence of $-NH_2$ groups at the open end of the PEG layer, as shown by the DLS data represented in Figure 4. In addition, a redshift from ∼520 nm (13 nm bare AuNP) to ∼525 nm without severe broadening in the UV−vis spectra also indicated successful PEG coating on AuNPs. PEGylated AuNP was modified with SPDP reagent, which was verified by the redshift in UV−vis spectra (from ∼525 nm (AuNP−PEG) to ∼527 nm (AuNP−PEG−SPDP)) and change in the surface charge (from +20 mV (AuNP−PEG) to +4 mV (AuNP−PEG−SPDP)). Following the SPDP modification, the thiol-siRNA (SH-siRNA) was attached to the AuNP−PEG−SPDP through the thiol−disulfide exchange reaction. Upon siRNA attachment, the zeta potential of the conjugates changed from positive (+4 mV) to slightly negative (−2.5 mV), cumulative size increased from ∼20 to ∼32 nm, and the maximum absorbance wavelength shifted from 527 to 534 nm (Figure 4). The conjugation yield of siRNA was calculated to be 56% (shown in the Supporting Information). The unconjugated siRNA was deliberately kept in the MCS solution and counted in siRNA dose calculations during transfection experiments. As the final step, siRNA-loaded AuNPs were electrostatically coated with TAT-HA2 peptide to complete AuNP-siRNA-Peptide MCS formation. The surface charge was altered from negative (−2.5 mV) to positive (+5 mV) through peptide coating due to the presence of cationic groups in the peptide structure. In addition, a slight increase in the size (from ∼32 to ∼46 nm) and shift in the maximum absorbance wavelength were observed upon the assembly of the peptide layer (Figure 4). After peptide addition, the complete system was purified using dialysis to remove excess peptides.

The RNase and serum stabilities of the AuNP-siRNA-Peptide MCSs were tested through a gel retardation assay (Figure 5A). The siRNA-loaded MCSs protected siRNA against both the RNase enzyme and serum proteins. There was no significant

https://doi.org/10.1021/acsomega.4c05808
ACS Omega 2024, 9, 47461−47474

intensity decrease above a 1:125 AuNP:Peptide ratio (or Peptide/siRNA ratio of 1.25).

The size of the multicomponent assembly, either in PBS or DMEM, did not change, while zeta potential values increased with the increased ratio of the AuNP/Peptide (Figure 5B,C). Positively charged particles in the PBS environment became negatively charged after incubation in DMEM due to the attachment of serum components (Figure 5B,C). The MCSs provided good RNase and serum stability above the Peptide/siRNA ratio of 1.25, while for the peptideplexes, the minimum ratio for siRNA stability was above 5. The results suggested that the MCSs require less peptide than the peptideplexes to protect the same amount of siRNA from degradation.

The cellular accumulation and time-dependent cellular uptake of MCSs were quantified by ICP-MS. Changing the AuNP/Peptide ratio from 1/125 to 1/500 (corresponding to a change in Peptide/siRNA ratio from 1.25 to 5) significantly increased the cellular accumulation of MCSs at the end of 24 h of incubation (Figure 6A). The increased peptide amount on the surface of MCSs provides free arginine residues, leading to enhanced cell membrane penetration and cellular entry.[32] The MCSs prepared with a AuNP/Peptide ratio of 1/500 (Peptide/siRNA ratio of 5) displayed slow cellular uptake within the first 30 min followed by dramatically enhanced uptake at 60 min. The uptaken MCSs appeared to provide a better endosomal escape ability (almost ∼70%; Figure 6C) than the peptideplexes (∼55%; Figure 3C) and were distributed in the cytoplasm. The better endosomal escape ability of MCSs is presumably due to the direct attachment of the peptide layer to the AuNP-PEG-siRNA conjugate surface, leading to better exposure of the fusogenic HA2 domains. Bulky complexation in the peptideplexes causes the embedding of active HA2 domains, preventing their exposure.[19,32−35,48] Contrary to the studies in the literature indicating the inefficient endosomal escape of the HA2 domain,[36,47] in the MCS approach, the synergistic effect of TAT and HA2 on endosomal escape ability was demonstrated. The results suggest that the distribution and availability of free HA2 domains on the surface of MCSs were potentially higher than in the case of peptideplexes, leading to a more efficient endosomal escape.

The transfection efficiency and toxicity of MCSs on the SKOV3 cell line were also evaluated. The MCSs without peptide (AuNP-siRNA) or siRNA alone did not display any gene silencing (luciferase suppression) effect. On the other hand, peptide-coating resulted in significant luciferase suppression without showing any toxic damage (Figure 7A and B). The luciferase suppression caused by the peptide-coated MCSs depended on the siRNA dose but did not significantly change with the AuNP/Peptide ratio or the Peptide/siRNA ratio (Figure 7A). At the Peptide/siRNA ratio of 5 with a 100 nm siRNA dose, the luciferase expression provided by the MCSs (AuNP/Peptide ratio of 1/500) was ∼55%, which was a ∼5% greater decrease than the commercial siRNA transfection reagent (Lipofectamine RNAiMax). With the same siRNA dose, the peptide complex formed at a Peptide/siRNA ratio of 10 decreased luciferase expression by ∼35% (Figure 3A). Consistent with our findings, previous studies also reported that MCSs have higher siRNA activity with lower siRNA loadings and lower toxicity than the complex siRNA delivery systems.[17,19,20,54−59] Higher amounts of siRNA and peptide are needed for peptideplexes to achieve similar gene silencing efficiency with MCSs, which may bring potential toxicity problems.[12]

The superior performance of MCSs could be due to the sterically advantageous placement of peptide molecules, allowing higher exposure of TAT and HA2 domains to cellular membranes and, hence, enhanced endosomal escape and distribution in the cytoplasm compared to the peptideplexes, in which active fractions of TAT and HA2 domains are possibly embedded in the complex structure. Additionally, the presence of cleavable disulfide bonds in MCSs structure may have facilitated the siRNA release, leading to higher activity over peptideplex counterparts with less peptide and siRNA loadings.[13,19,20,54−57]

3.3. Peptide−siRNA Conjugate System. The third siRNA delivery system developed in this study was a conjugate system formed based on the covalent attachment of thiol-modified siRNA to the peptides through the cleavable disulfide bonds using a multifunctional cross-linker (SPDP). Following the modification of the peptide amine groups with the SPDP linker, thiol-modified siRNA was conjugated with the SPDP-modified peptide through the thiol−disulfide exchange reaction, leading to the formation of disulfide bonds between the peptide and siRNA. The disulfide bonds were expected to be reduced and facilitate siRNA release in the cytoplasm. Before all experiments, the unconjugated siRNA and peptide residues were removed from the conjugate using dialysis, as mentioned in Section 2.4. The successful synthesis of the Peptide−siRNA conjugate was confirmed by cleaving the formed disulfide bonds using TCEP. The released siRNA amount was ∼15 μM, corresponding to a conjugation efficiency of ∼75%. The agarose gel electrophoresis also demonstrated successful conjugation (Figure 8A).

The complete siRNA retardation was observed for the conjugates formed at Peptide/siRNA ratios of 7.5 and 10. In contrast, the mobilities of free siRNA and the conjugate prepared at a Peptide/siRNA ratio of 5 on the gel were found to be similar (Figure 8A). The conjugate prepared at the Peptide/siRNA ratio of 5 showed dissociation after serum incubation, while conjugates formed at 7.5 and 10 stayed stable against serum proteins by not migrating on the gel (Figure 8B). Only the conjugate prepared at the Peptide/siRNA ratio of 10 showed significant protection against the RNase enzyme. The RNase stabilities of other conjugates were found to be low, showing drastically little illumination on the gel (Figure 8C). The amine groups on peptide molecules were modified with uncharged SPDP groups, leading to incomplete coverage of siRNA by peptide molecules and leaving siRNA strands open to external effects. This situation could be eliminated by coating the surface of the conjugate with a small amount of nonmodified peptide to provide a shielding effect.

The conjugate sizes in the PBS buffer and DMEM remained between the peptideplexes and MCSs and slightly increased with the Peptide/siRNA ratio. The size was slightly larger in serum-containing DMEM than in PBS, possibly due to the adsorption of serum components (Figure 8D). Like the other systems, the conjugates also had a positive charge in PBS buffer, which turned negative upon incubation in serum-containing DMEM, indicating the binding of negatively charged serum components (Figure 8E). The conjugates' cellular uptake and endosomal escape capabilities could not be evaluated since, after SPDP modification and siRNA conjugation, there are no more available functional groups on peptide molecules for fluorescence dye attachment. However, the effective luciferase activity of the conjugates indirectly proved the cellular uptake and endosomal escape ability of the conjugates.

https://doi.org/10.1021/acsomega.4c05808
ACS Omega 2024, 9, 47461−47474

At the maximum dose (200 nM), the conjugate systems reduced the luciferase expression to ∼35% regardless of the Peptide/siRNA ratio, without showing severe toxicity (Figure 9A,B). However, the gene silencing efficiencies decreased significantly as the dose was reduced to 50 nM. With the Peptide/siRNA ratio of 10 and siRNA dose of 100 nM, the conjugate showed similar luciferase activity to the commercial siRNA carrier, RNAiMax, higher activity than the peptideplex, and ∼10% less luciferase suppression than MCS possessing a AuNP/Peptide ratio of 1/500. The better performance of conjugates in luciferase suppression activity without any toxicity over their peptideplex counterparts could be mainly attributed to disulfide bonds that enable the efficient endosomal escape and cytosolic release of siRNA molecules. Additionally, the covalent conjugation may allow better exposure of the TAT and HA2 domains to show activity in enhancing cellular entry and endosomal escape, respectively. The electrostatic interactions in the peptide complexes may restrict the performance of TAT and HA2 domains on cellular membranes and fail to provide efficient endosomal escape of siRNA molecules. Although the luciferase suppression activities of conjugate and MCS systems were found to be similar at the same siRNA dose, the one-step conjugation of siRNA to peptide in conjugate systems could be advantageous considering the multiple steps in the preparation of MCSs.

Based on the presented results, a direct comparison between the developed and tested systems was presented in Figure 10A,B based on 100 nM of applied siRNA dose. The results indicated that the multicomponent and conjugate systems provided better luciferase expression suppression with minimal toxicity. However, it should be noted that the slight toxic effect of the conjugate system (∼80% cell viability) could contribute to the high luciferase expression suppression of the conjugate system. In Figure 10, these systems were also compared with the RNAiMax with luciferase-suppressing siRNA and negative control, scrambling siRNA. The results indicated that the multicomponent and conjugate systems showed similar transfection efficacy with the RNAiMax/Luc-siRNA but showed better efficacy than the RNAiMax/NC-siRNA. Standard *t*-test was applied to identify the statistical significance.

4. CONCLUSION

This study compared the efficacy of the TAT-HA2 peptide in peptideplex, multicomponent, and conjugate-based siRNA delivery systems. The results indicated that except for the peptideplexes prepared with a Peptide/siRNA ratio of 5 and conjugate systems with 5 and 7.5, all delivery systems maintained particulate stability (size and zeta potential) in serum-supplemented cell culture media and protected siRNA from RNase and serum proteins. The surface attachment of peptides in MCSs and the direct conjugation of siRNA to peptides revealed the advantages of each domain. In contrast, the possible embedding of active domains into the peptide-plex matrix restricted their favorable properties. Accordingly, endosomal escape capabilities of multicomponent systems were noted to be better than those of the peptideplexes, contributing to their higher transfection efficiencies. The cleavable disulfide bonds in multicomponent and conjugate systems promoted siRNA release in the cytoplasm, enhancing the transfection efficiency. However, the strong electrostatic interactions in peptide complexes prevented efficient siRNA release and activity in the cytoplasm. The siRNA activities of the multicomponent and conjugate systems were similar and ∼25% and 5% higher than those of peptideplexes and commercial RNAiMax at the same applied dose, respectively. To achieve the same level of luciferase activity, the siRNA loading was reported to be four times lower in the multicomponent and conjugate systems than in the peptideplex systems, which also brought about lower peptide usage in multicomponent and conjugate systems. None of the developed systems showed significant toxicity at any dose. Overall, it can be concluded that the TAT-HA2 cell-penetrating and fusogenic peptides are promising vectors to deliver siRNA, especially when used in multicomponent and conjugate systems, highlighting the advantage of each peptide domain better.

■ ASSOCIATED CONTENT

Supporting Information

The Supporting Information is available free of charge at https://pubs.acs.org/doi/10.1021/acsomega.4c05808.

Calculation of SPDP modification; calculation of NHS-fluorescein labeling degree of peptides; calculation of number of AuNPs per cell by ICP-MS analysis; theoretical siRNA loading on 20 nM AuNPs; experimental siRNA loading on 20 nM AuNP solution (PDF)

■ AUTHOR INFORMATION

Corresponding Author

Metin Uz − *Department of Chemical and Biomedical Engineering, Cleveland State University, Cleveland, Ohio 44115-2214, United States;* orcid.org/0000-0003-0341-9264; Phone: +1216 687 3526; Email: m.uz@csuohio.edu

Authors

Volga Bulmus − *Department of Bioengineering, Izmir Institute of Technology, Izmir 35430, Turkey;* orcid.org/0000-0001-9944-1444

Sacide Alsoy Altinkaya − *Department of Chemical Engineering, Izmir Institute of Technology, Izmir 35430, Turkey;* orcid.org/0000-0002-7049-7425

Complete contact information is available at: https://pubs.acs.org/10.1021/acsomega.4c05808

Notes

The authors declare no competing financial interest.

■ ACKNOWLEDGMENTS

We acknowledge the Cleveland State University the Office of Research Faculty Research and Development (FRD) Program, the Washkewicz College of Engineering, and the Department of Chemical and Biomedical Engineering for providing funding. We also acknowledge The Scientific and Technological Research Council of Turkey (TÜBİTAK) Graduate Scholarship Program and Izmir Institute of Technology (grant # 2009IYTE01) for their support, as well as the Biotechnology/Bioengineering, Environmental, and Materials Research Centers at Izmir Institute of Technology for providing facilities.

■ REFERENCES

(1) Resnier, P.; et al. A review of the current status of siRNA nanomedicines in the treatment of cancer. *Biomaterials* **2013**, *34* (27), 6429−6443.

(2) Bora, R. S.; Gupta, D.; Mukkur, T. K. S.; Saini, K. S. RNA interference therapeutics for cancer: Challenges and opportunities (Review). *Mol. Med. Rep.* **2012**, *6* (1), 9−15.

(3) Shrey, K.; et al. RNA interference: Emerging diagnostics and therapeutics tool. *Biochem. Biophys. Res. Commun.* **2009**, *386* (2), 273−277.
(4) Devi, G. R. siRNA-based approaches in cancer therapy. *Cancer Gene Ther.* **2006**, *13* (9), 819−829.
(5) Charbe, N.; et al. Small interfering RNA for cancer treatment: overcoming hurdles in delivery. *Acta Pharm. Sin. B* **2020**, *10*, 2075−2109.
(6) Goyal, R.; Chopra, H.; singh, I.; Dua, K.; Gautam, R. K. Insights on prospects of nano-siRNA based approaches in treatment of Cancer. *Front. Pharmacol.* **2022**, *13*, 985670.
(7) Hattab, D.; Gazzali, A. M.; Bakhtiar, A. Clinical Advances of siRNA-Based Nanotherapeutics for Cancer Treatment. *Pharmaceutics* **2021**, *13* (7), 1009.
(8) Scholz, C.; Wagner, E. Therapeutic plasmid DNA versus siRNA delivery: Common and different tasks for synthetic carriers. *J. Controlled Release* **2012**, *161* (2), 554−565.
(9) Zhang, J.; et al. A Comprehensive Review of Small Interfering RNAs (siRNAs): Mechanism, Therapeutic Targets, and Delivery Strategies for Cancer Therapy. *Int. J. Nanomed.* **2023**, *18*, 7605−7635.
(10) Elbakry, A.; et al. Layer-by-Layer Coated Gold Nanoparticles: Size-Dependent Delivery of DNA into Cells. *Small* **2012**, *8* (24), 3847−3856.
(11) Elbakry, A.; et al. Layer-by-Layer Assembled Gold Nanoparticles for siRNA Delivery. *Nano Lett.* **2009**, *9* (5), 2059−2064.
(12) Ballarin-Gonzalez, B.; Howard, K. A. Polycation-based nanoparticle delivery of RNAi therapeutics: Adverse effects and solutions. *Adv. Drug Delivery Rev.* **2012**, *64* (15), 1717−1729.
(13) Varkouhi, A. K.; et al. Polyplexes based on cationic polymers with strong nucleic acid binding properties. *Eur. J. Pharm. Sci.* **2012**, *45* (4), 459−466.
(14) Dong, Y.; Siegwart, D.; Anderson, D. Strategies, design, and chemistry in siRNA delivery systems. *Adv. Drug Delivery Rev* **2019**, *144*, 133−147.
(15) Tatiparti, K.; Sau, S.; Kashaw, S. K.; Iyer, A. K. siRNA Delivery Strategies: A Comprehensive Review of Recent Developments. *Nanomaterials* **2017**, *7*, 77.
(16) Wang, J.; Chen, G.; Liu, N.; Han, X.; Zhao, F.; Zhang, L.; Chen, P. Strategies for improving the safety and RNAi efficacy of noncovalent peptide/siRNA nanocomplexes. *Adv. Colloid Interface Sci.* **2022**, *302*, 102638.
(17) Gunasekaran, K.; et al. Conjugation of siRNA with Comb-Type PEG Enhances Serum Stability and Gene Silencing Efficiency. *Macromol. Rapid Commun.* **2011**, *32* (8), 654−659.
(18) Lytton-Jean, A. K. R.; Langer, R.; Anderson, D. G. Five Years of siRNA Delivery: Spotlight on Gold Nanoparticles. *Small* **2011**, *7* (14), 1932−1937.
(19) Uz, M.; Mallapragada, S. K.; Altinkaya, S. A. Responsive pentablock copolymers for siRNA delivery. *RSC Adv.* **2015**, *5* (54), 43515−43527.
(20) Lee, J. S.; et al. Gold, Poly(beta-amino ester) Nanoparticles for Small Interfering RNA Delivery. *Nano Lett.* **2009**, *9* (6), 2402−2406.
(21) Lee, M. Y.; et al. Target-Specific Gene Silencing of Layer-by-Layer Assembled Gold-Cysteamine/siRNA/PEI/HA Nanocomplex. *ACS Nano* **2011**, *5* (8), 6138−6147.
(22) Dong, W. J.; Zhou, Y. J.; Liang, W. Lipid-based siRNA Delivery Systems. *Prog. Biochem. Biophys.* **2012**, *39* (5), 396−401.
(23) Hoyer, J.; Neundorf, I. Peptide Vectors for the Nonviral Delivery of Nucleic Acids. *Acc. Chem. Res.* **2012**, *45* (7), 1048−1056.
(24) Liu, X. Q.; et al. Polymeric-Micelle-Based Nanomedicine for siRNA Delivery. *Part. Part. Syst. Charact.* **2013**, *30* (3), 211−228.
(25) Nakase, I.; Tanaka, G.; Futaki, S. Cell-penetrating peptides (CPPs) as a vector for the delivery of siRNAs into cells. *Mol. BioSyst.* **2013**, *9* (5), 855−861.
(26) Wu, Z. W.; et al. Recent progress in copolymer-mediated siRNA delivery. *J. Drug Targeting* **2012**, *20* (7), 551−560.
(27) Kesharwani, P.; Gajbhiye, V.; Jain, N. K. A review of nanocarriers for the delivery of small interfering RNA. *Biomaterials* **2012**, *33* (29), 7138−7150.
(28) Lee, J.-M.; Yoon, T.-J.; Cho, Y.-S. Recent Developments in Nanoparticle-Based siRNA Delivery for Cancer Therapy. *Biomed Res. Int.* **2013**, *2013*, 782041.
(29) Li, J.; et al. Recent advances in delivery of drug-nucleic acid combinations for cancer treatment. *J. Controlled Release* **2013**, *172* (2), 589−600.
(30) Tai, W.; Gao, X. Functional peptides for siRNA delivery. *Adv. Drug Delivery Rev.* **2017**, *110*, 157−168.
(31) Singh, T.; Murthy, A. S. N.; Yang, H.-J.; Im, J. Versatility of cell-penetrating peptides for intracellular delivery of siRNA. *Drug Delivery* **2018**, *25*, 1996−2006.
(32) Wadia, J. S.; Stan, R. V.; Dowdy, S. F. Transducible TAT-HA fusogenic peptide enhances escape of TAT-fusion proteins after lipid raft macropinocytosis. *Nat. Med.* **2004**, *10* (3), 310−315.
(33) Lee, Y. J.; Johnson, G.; Pellois, J. P. Modeling of the Endosomolytic Activity of HA2-TAT Peptides with Red Blood Cells and Ghosts. *Biochemistry* **2010**, *49* (36), 7854−7866.
(34) Sugita, T.; et al. Improved cytosolic translocation and tumor-killing activity of Tat-shepherdin conjugates mediated by co-treatment with Tat-fused endosome-disruptive HA2 peptide. *Biochem. Biophys. Res. Commun.* **2007**, *363* (4), 1027−1032.
(35) Ye, S. F.; et al. Synergistic effects of cell-penetrating peptide Tat and fusogenic peptide HA2-enhanced cellular internalization and gene transduction of organosilica nanoparticles. *Nanomed.-Nanotechnol. Biol. Med.* **2012**, *8* (6), 833−841.
(36) Cesbron, Y.; et al. TAT and HA2 facilitate cellular uptake of gold nanoparticles but do not lead to cytosolic localisation. *PLoS One* **2015**, *10* (4), No. e0121683.
(37) Ye, S.; et al. Tat/HA2 Peptides Conjugated AuNR@pNIPAAm as a Photosensitizer Carrier for Near Infrared Triggered Photodynamic Therapy. *Mol. Pharmaceutics* **2015**, *12* (7), 2444−2458.
(38) Turkevich, J.; Stevenson, P. C.; Hillier, J. A study of the nucleation and growth processes in the synthesis of colloidal gold. *Discuss. Faraday Soc.* **1951**, *11*, 55.
(39) Hakkinen, H. The gold-sulfur interface at the nanoscale. *Nat. Chem.* **2012**, *4* (6), 443−455.
(40) Gu, Y. J.; et al. Nuclear penetration of surface functionalized gold nanoparticles. *Toxicol. Appl. Pharmacol.* **2009**, *237* (2), 196−204.
(41) Zhang, S. B.; et al. Cationic lipids and polymers mediated vectors for delivery of siRNA. *J. Controlled Release* **2007**, *123* (1), 1−10.
(42) Armstrong, J.; et al. The hydrodynamic radii of macromolecules and their effect on red blood cell aggregation. *Biophys. J.* **2004**, *87*, 4259−4270.
(43) Nicholson, J.; Wolmarans, M.; Park, G. The role of albumin in critical illness. *Br. J. Anaesth.* **2000**, *85*, 599−610.
(44) Vandenbroucke, R. E.; et al. Cellular entry pathway and gene transfer capacity of TAT-modified lipoplexes. *Biochim. Biophys. Acta, Biomembr.* **2007**, *1768* (3), 571−579.
(45) Brooks, H.; Lebleu, B.; Vives, E. Tat peptide-mediated cellular delivery: back to basics. *Adv. Drug Delivery Rev.* **2005**, *57* (4), 559−577.
(46) Varkouhi, A. K.; et al. Endosomal escape pathways for delivery of biologicals. *J. Controlled Release* **2011**, *151* (3), 220−228.
(47) Lee, Y. J.; et al. A HA2-Fusion tag limits the endosomal release of its protein cargo despite causing endosomal lysis. *Biochim. Biophys. Acta, Gen. Subj.* **2011**, *1810* (8), 752−758.
(48) Liou, J. S.; et al. Protein transduction in human cells is enhanced by cell-penetrating peptides fused with an endosomolytic HA2 sequence. *Peptides* **2012**, *37* (2), 273−284.
(49) Hoyer, J.; Neundorf, I. Knockdown of a G protein-coupled receptor through efficient peptide-mediated siRNA delivery. *J. Controlled Release* **2012**, *161* (3), 826−834.
(50) Lee, S. H.; Kim, S. H.; Park, T. G. Intracellular siRNA delivery system using polyelectrolyte complex micelles prepared from VEGF siRNA-PEG conjugate and cationic fusogenic peptide. *Biochem. Biophys. Res. Commun.* **2007**, *357* (2), 511−516.
(51) Mok, H.; Park, T. G. Self-crosslinked and reducible fusogenic peptides for intracellular delivery of siRNA. *Biopolymers* **2008**, *89* (10), 881−888.

https://doi.org/10.1021/acsomega.4c05808
ACS Omega 2024, 9, 47461−47474

(52) Oliveira, S.; et al. Fusogenic peptides enhance endosomal escape improving siRNA-induced silencing of oncogenes. *Int. J. Pharm.* **2007**, *331* (2), 211−214.
(53) Rodrigues, F.; Darbre, T.; Machuqueiro, M. High Charge Density in Peptide Dendrimers is Required to Destabilize Membranes: Insights into Endosome Evasion. *J. Chem. Inf. Model.* **2024**, *64*, 3430−3442.
(54) Cheng, R.; et al. Glutathione-responsive nano-vehicles as a promising platform for targeted intracellular drug and gene delivery. *J. Controlled Release* **2011**, *152*, 2−12.
(55) Giljohann, D. A.; Seferos, D. S.; Prigodich, A. E.; Patel, P. C.; Mirkin, C. A. Gene Regulation with Polyvalent siRNA−Nanoparticle Conjugates. *J. Am. Chem. Soc.* **2009**, *131* (6), 2072−2073.
(56) Lee, S.; et al. Amine-functionalized gold nanoparticles as non-cytotoxic and efficient intracellular siRNA delivery carriers. *Int. J. Pharm.* **2008**, *364*, 94−101.
(57) Oishi, M.; Nakaogami, J.; Ishii, T.; Nagasaki, Y. Smart PEGylated gold nanoparticles for the cytoplasmic delivery of siRNA to induce enhanced gene silencing. *Chem. Lett.* **2006**, *35*, 1046−1047.
(58) Takemoto, H.; Ishii, A.; Miyata, K.; Nakanishi, M.; Oba, M.; Ishii, T.; Yamasaki, Y.; Nishiyama, N.; Kataoka, K. Polyion complex stability and gene silencing efficiency with a siRNA-grafted polymer delivery system. *Biomaterials* **2010**, *31*, 8097−8105.
(59) Varkouhi, A. K.; Verheul, R. J.; Schiffelers, R. M.; Lammers, T.; Storm, G.; Hennink, W. E. Gene Silencing Activity of siRNA Polyplexes Based on Thiolated N,N,N-Trimethylated Chitosan. *Bioconjugate Chem.* **2010**, *21*, 2339−2346.

https://doi.org/10.1021/acsomega.4c05808
ACS Omega 2024, 9, 47461−47474